Bloch, W., Schurr, B., Kummerow, J., Salazar, P., Shapiro, S. A. (2018): From Slab Coupling to Slab Pull: Stress Segmentation in the Subducting Nazca Plate. - *Geophysical Research Letters*, *45*, 11, pp. 5407—5416.

DOI: http://doi.org/10.1029/2018GL078793

Geophysical Research Letters

RESEARCH LETTER
10.1029/2018GL078793

Key Points:
- We find a systematic segmentation of focal mechanisms of moderate earthquakes in a subducting slab
- We observe the sharp downdip termination of the locked zone of the plate interface
- Slab pull stresses are not fully transferred from below 100 km to the shallower parts of the slab

Supporting Information:
- Supporting Information S1

Correspondence to:
W. Bloch,
wasja@gfz-potsdam.de

Citation:
Bloch, W., Schurr, B., Kummerow, J., Salazar, P., & Shapiro, S. A. (2018). From slab coupling to slab pull: Stress segmentation in the subducting Nazca plate. *Geophysical Research Letters*, *45*, 5407–5416. https://doi.org/10.1029/2018GL078793

Received 16 MAY 2018
Accepted 18 MAY 2018
Accepted article online 29 MAY 2018
Published online 12 JUN 2018

From Slab Coupling to Slab Pull: Stress Segmentation in the Subducting Nazca Plate

Wasja Bloch[1,2], Bernd Schurr[2], Jörn Kummerow[1], Pablo Salazar[3,4], and Serge A. Shapiro[1]

[1]Institut für Geologische Wissenschaften, Freie Universität Berlin, Berlin, Germany, [2]Deutsches GeoForschungszentrum Potsdam, Potsdam, Germany, [3]Departamento de Ciencias Geológicas, Universidad Católica del Norte, Antofagasta, Chile, [4]National Research Center for Integrated Natural Disasters Management (CIGIDEN), Santiago, Chile

Abstract We investigate the stress field that the Nazca slab experiences during subduction beneath the South American plate by determining the focal mechanisms of moderate subduction-related earthquakes continuously from 20- to 120-km depth and inverting for the stress directions of four slab regions. Our results show the sharp termination of the coupling zone, which is characterized by compressional stresses, uplift of the overlying mountain range, and likely the activation of preexisting slab structures. Beyond and below this zone slab pull is the dominant stress. Near the slab surface, we also find signatures of the activation of inherited structures. Deeper in the slab, fault orientations are more likely controlled by the stress field alone. Along the subduction pathway, we find indication for an increase of the absolute slab pull component of the stress field that correlates with an increase in event rate and the occurrence possibility of $M > 7$ intermediate depth earthquakes.

Plain Language Summary We investigated the sense of movement and the orientation of ruptures of moderate earthquakes that occur in the part of the Nazca tectonic plate which sinks below the South American tectonic plate. We aim to better understand why and how tectonic plates sink into the Earth. Our research shows that the earthquakes on top of the Nazca plate to about 50-km depth occur, because both plates partially stick together in their movement against each other. Below 50-km depth, the sticking together ends and the deepest part of the Nazca plate pulls on the shallower part, likely because there it is heavier. We discovered that the pulling becomes stronger below 100-km depth, and we think that this is one aspect of why at this depth there are more and potentially very strong earthquakes. Our research also shows that ruptures that were mapped on the ocean floor are likely still there when the tectonic plate sinks into the Earth but that they do not reach deeper than approximately 12 km into the plate. With this knowledge we can start to estimate how heavy the plate is at which depth, where the pulling starts, and what contributes to it.

1. Introduction

In the Central Andean subduction zone around 21°S the Nazca plate subducts beneath the South American Plate with a velocity of 67 mm/year in a direction of N77°E (Angermann et al., 1999; Figure 1). Upon subduction the plate bends and develops bend faults in the outer rise region (Ranero et al., 2003, 2005). At depth, the slab unbends to subduct at a constant dip of ~ 20° to a depth of about 120 km (Sippl et al., 2018; Wölbern et al., 2009; Yuan et al., 2000). Slab-related seismicity has the form of three slab-parallel planes (Bloch et al., 2014). The upper plane traces the plate interface, while the middle plane is located close to the oceanic Moho and the lower plane ~30 km below in the oceanic mantle (Figure 1). The two lower planes merge in a strong seismicity cluster below the magmatic arc at ~100-km depth, which forms a narrow double seismic zone (Comte & Suarez, 1994; Rietbrock & Waldhauser, 2004) and can produce $M7-8$ intermediate depth earthquakes (Delouis & Legrand, 2007; Kausel & Campos, 1992; Peyrat et al., 2006). It has been hypothesized that the strong seismicity cluster is the locus of major slab devolatilization (e.g., Oncken et al., 1999). In agreement with this hypothesis, active source seismic data revealed a prominent reflective structure above the cluster that likely represents a conduit through which fluids rise toward the surface, causing melting and arc volcanism (Oncken et al., 2003; Yoon et al., 2008). Furthermore, beyond the strong cluster the slab becomes transparent in receiver function images (Wölbern et al., 2009; Yuan et al., 2000) and the deeper seismicity indicates a steepening of the slab (Sippl et al., 2018). Both observations may be explained with a density increase

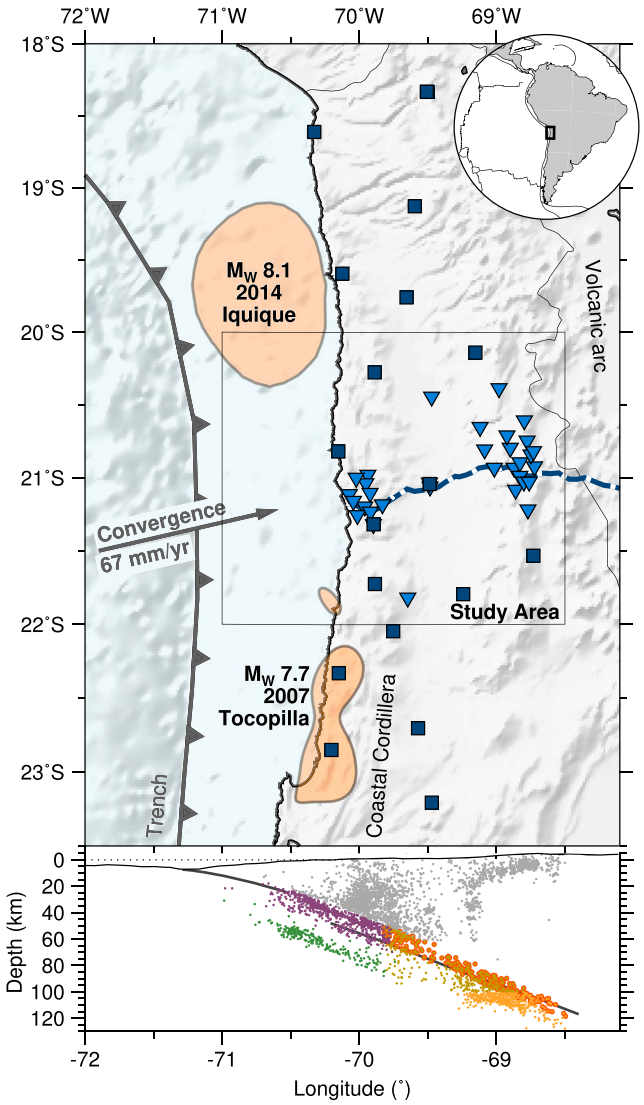

Figure 1. The study area in northern Chile, including seismic networks. (top) Map view with Peru-Chile trench (jagged line), convergence vector (Angermann et al., 1999), rupture areas of the 2014 Iquique (Schurr et al., 2014) and the 2007 Tocopilla (Schurr et al., 2012) megathrust earthquakes (orange patches), temporary short-period seismic network (blue triangles, FDSN code: 8F; Wigger et al., 2016), permanent broadband seismic network (blue squares, FDSN code: CX; GFZ, and IPGP, 2006), seismic profile (dashed line; Lüth, 2000; Oncken et al., 1999; Yoon et al., 2008). (bottom) E-W profile with seismicity (color coded by regions discussed in the text; events that are outlined orange red occur within ~12 km below the plate interface; Bloch et al., 2014). Slab 1.0 model of the slab surface (black line toward the trench; Hayes et al., 2012) and negative receiver function signature of the slab Moho (black line toward the arc; Yuan et al., 2000).

that would be due to the eclogitization of oceanic crust and/or the deserpentinization of the oceanic mantle at the depth of the seismicity cluster.

At shallow depth, convergence along the locked plate boundary accumulates strain that is periodically released in megathrust earthquakes. Recently, the M_w8.1, 2014 Iquique earthquake (Hayes et al., 2014; Ruiz et al., 2014; Schurr et al., 2014) ruptured the segment north of the study area, between ~ 19.0°S and 20.5°S and the M_w7.7, 2007 Tocopilla earthquake (Delouis et al., 2009; Schurr et al., 2012) ruptured the segment to the south, between ~ 22°S and 23°S (Figure 1). The segment within the study area and south of it, reaching at least from 20.5°S to ~ 22°S, has not been activated since the M_L8.6, 1877 Iquique earthquake (Comte & Pardo, 1991). Based on Global Positioning System (GPS) measurements of the interseismic surface strain field, it has been suggested that the study area is located at a seismotectonic barrier that may limit the rupture length of a forthcoming megathrust earthquake (Métois et al., 2013).

Focal mechanisms of subduction related earthquakes in this tectonically highly active region have so far only been inferred from the analysis of *P* wave first motion polarities. Above ~50-km depth, some of the found mechanisms may represent slip on the plate interface (Comte et al., 1999; Delouis et al., 1996). Downdip, the slab is under tension (Comte et al., 1999; Delouis et al., 1996; Rietbrock & Waldhauser, 2004) and it has been hypothesized that some of the earthquakes may reactivate outer rise bend faults (Ranero et al., 2005; Rietbrock & Waldhauser, 2004).

Here we continue to study the stresses that act on the slab by evaluating the focal mechanisms of moderate earthquakes ($2 < M_l < 5$) and inverting for stress directions (e.g., Kumar et al., 2016) within the slab and at its interface to the upper plate in the Central Andean subduction zone. We take advantage of the detailed knowledge about the subsurface velocity structure (Husen et al., 1999; Lüth, 2000), the dense and widespread instrumentation of the study area (Figure 1), and the accurate event locations (Bloch et al., 2014) that allow here for the calculation of precise focal mechanisms, even for the weaker, previously undetected events. The clear development of a triple seismic zone allows us to sample the stresses continuously along and across the slab, from 20- to 120-km depth, in the oceanic crust and mantle. The relatively simple subduction geometry yields an unveiled view on the underlying processes.

2. Data and Method

We used seismograms that have been recorded by the temporary short-period seismic network 8F (Wigger et al., 2016) and the permanent broadband network CX (GFZ, and IPGP, 2006) in the time span between March 2010 and March 2012 (Figure 1), in the late interseismic phase before the 2014 Iquique earthquake. For 152 earthquakes, we inverted for the parameters of a double couple (DC) source using the *HASH* algorithm (Hardebeck & Shearer, 2002, 2003). We confirmed the focal mechanism of 10 of the strongest events down to a magnitude M_w3.5 using the full waveform inversion algorithm *RMT* (Nábělek & Xia, 1995) and inverted for stress directions using the *slick* algorithm (Gephart & Forsyth, 1984; Michael, 1987).

For the inversion with HASH, we used *P* wave first motion polarities and *P* to *S* amplitude ratios. We determined the *P* polarities on the unfiltered short period or the 1 Hz high-pass filtered broadband-integrated vertical displacement seismograms and the maximum *P* and *S* amplitudes on the Cartesian sum trace of all three components. We computed takeoff angles in a 2-D velocity model that was obtained using wide-angle active source seismic data from a profile across our study area (Lüth, 2000; Figure 1). We then used HASH to invert for the orientation of a DC source that best matches the observed radiation pattern. We assessed the stability of the results by reperforming the inversion with takeoff angles perturbed with a standard deviation of 5° (supporting information S1).

We confirmed 10 of the mechanisms by inverting the full waveform (supporting information S2). To do so, we computed elastodynamic Green's functions (Bouchon, 1981) using a 1-D velocity model that was generated from arrival time inversion of the aftershock sequence of the M_w8.0, 1995 Antofagasta earthquake (Husen et al., 1999). We used the source parameters of the HASH solution as a starting source mechanism and performed an interactive full waveform inversion of the restituted displacement seismograms, which were band-pass filtered between 2 and 20 s for stronger events and 0.5 and 5 s for weaker events. The filter bands were individually chosen so as to minimize the influence of unmodeled structure, noise, and microseisms on the seismograms. For the fixed far-field source time function we always used a simple pulse-like triangle function with half duration of 0.2 s. For a specific magnitude and frequency band the source duration should most probably be below the applied short-period filter corner and therefore not influence the seismograms. We tested the source time function to perform well for the range of observed magnitudes. We constrained the moment tensor not to contain a volumetric component. We note that the compensated linear vector dipole component of the moment tensor (e.g., Jost & Herrmann, 1989) increases, the further the hypocenter is located away from ~50-km depth and 70°W, which is the region for which the 1-D velocity model of Husen et al. (1999) has been optimized and where it therefore should approximate the real subsurface structure best. In a suite of synthetic tests Schurr and Nábělek (1999) showed that the compensated linear vector dipole component may become artificially large when unmodeled subsurface structures are present. We therefore only interpreted the DC component of the moment tensors.

We inspected the resulting focal mechanisms for robustness, uniqueness, and coherence with the data. Based on these categories, we assigned three different qualities: (A) RMT moment tensor which is consistent with the starting model, (B) HASH focal mechanism with a well covered focal sphere and internally consistent polarities

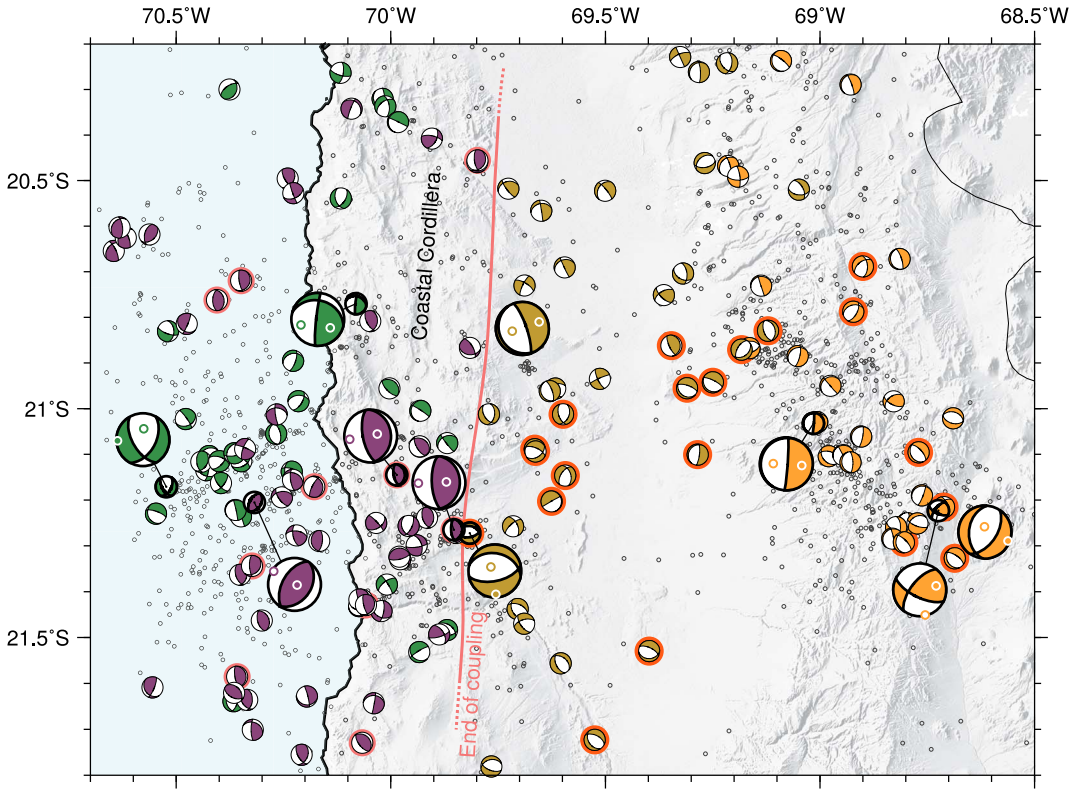

Figure 2. Topographic map view of the study area showing focal mechanisms of earthquakes within the subducting Nazca slab or along the plate boundary. Large focal mechanisms with thick outlines and *P*/*T* axes are constrained by full waveform inversion (all *P*/*T* axes in Figure 3). Color code as is Figure 1. Salmon red line indicates the region on the plate interface where interface thrust events (outlined in salmon red) occur.

and *P*/*S* amplitude ratios, and (C) HASH focal mechanism where the type of faulting (normal, reverse, or strike-slip) is constrained but where either the focal sphere is only poorly covered or some of the observations are inconsistent. The overall pattern of the stress field remains stable, independent of whether we include (B) or (C) quality focal mechanisms (supporting information S3). Focal mechanisms that could not be resolved or were ambiguous were not considered.

We separated the found focal mechanisms into four regions guided by the structure of the subducting slab (Figure 1, profile): The upper two planes of seismicity (purple in Figures 1–3), the lower plane of seismicity (green), a transitional zone beyond the downdip end of interface seismicity (brown), and the strong seismicity cluster (orange, depth > 100 km). For each region we inverted for the orientation of the principal stresses ($\sigma_1 \geq \sigma_2 \geq \sigma_3$) and the shape parameter $\Phi = \frac{\sigma_2-\sigma_3}{\sigma_1-\sigma_3}$ using the slick algorithm. We determined the 95% confidence limits of all parameters by bootstrapping (Gephart & Forsyth, 1984; Michael, 1987). We assumed that all absolute stresses are compressive and that compressive stresses are positive (supporting information S4).

3. Results

The DC part of the moment tensors plotted as beach balls are shown in Figure 2, the corresponding *P*, *N*, and *T* axes distributions and the orientation of the principal stresses in Figure 3.

The earthquakes of the upper two planes have mostly reverse faulting mechanisms. A group of them is characterized by shallow thrust on a ~ 20°E dipping plane. This group very likely represents seismic slip on the plate interface (interface thrust, outlined salmon red in Figure 2 and *IT* in Figure 3). The group is well constrained by two quality (A) focal mechanisms. The other reverse faulting events in the upper seismicity planes have nodal planes that dip significantly steeper than the plate interface. σ_1 is oriented near horizontal in convergence direction and σ_3 near vertical.

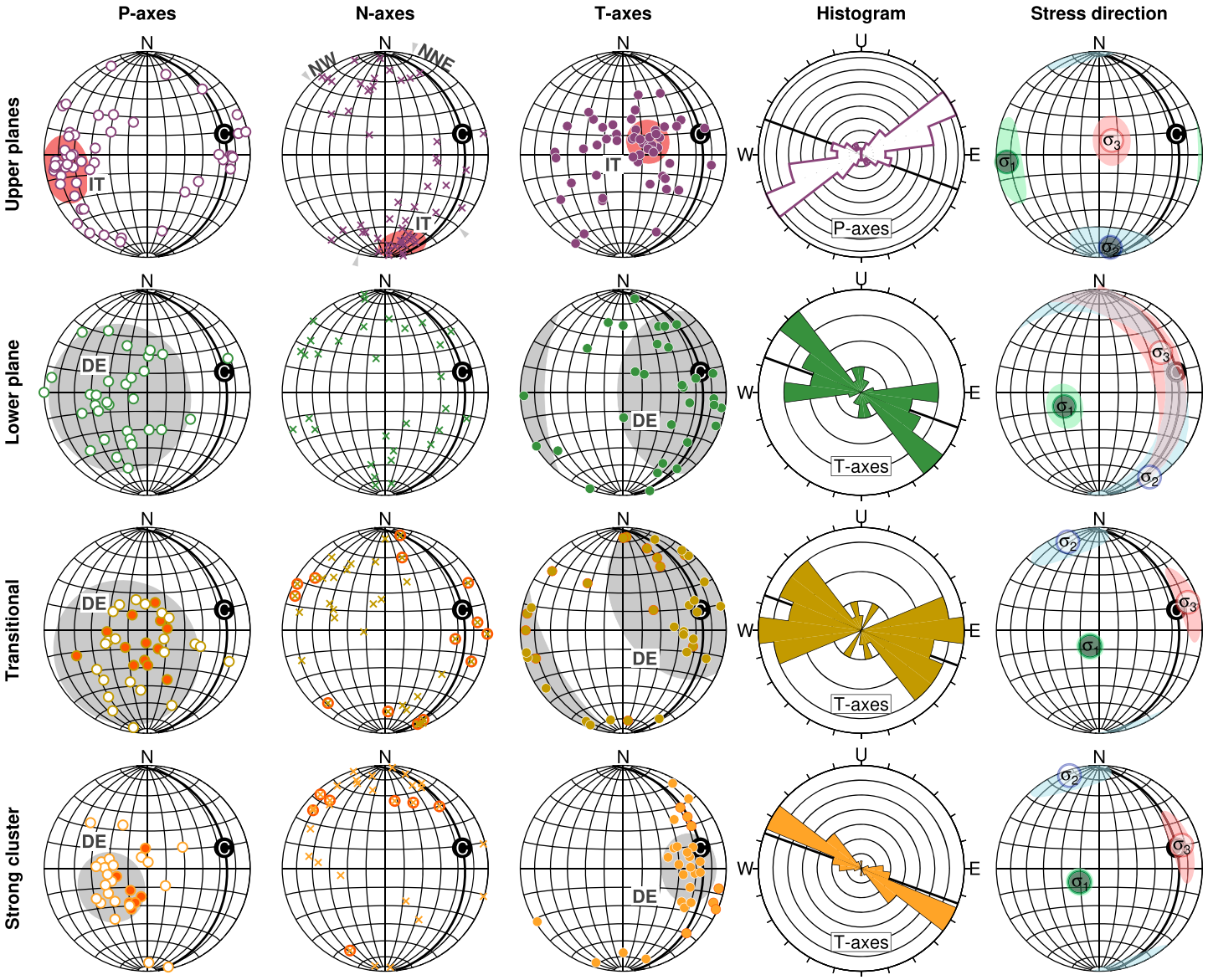

Figure 3. Lower hemisphere stereographic projections of the *P*, *N*, and *T* axes (first three columns, shaded areas indicate clustering of axes discussed in the text. IT: interface thrust. DE: downdip extension. NW and NNE: direction of mapped outer rise bend faults; Ranero et al., 2005), polar histogram of the *P* or *T* axes orientation in the profile plane (fourth column, bin width 15°, concentric lines at intervals of two events, all color coded by region as in Figure 1), and stress directions (last column, error ellipsoids indicate 95% confidence region; dark and light fill indicate compressive and extensive relative stresses. Stress directions and Phi are tabled in the supporting information, where Phi is the greek capital letter.) C: Downdip convergence direction. Black line: Slab plane.

An abrupt change in faulting style occurs at the downdip end of seismicity along the plate interface at 69.85°W, 21.30°S, 55-km depth (Figures 2 and 4). At this point, a typical interface thrust event occurs less than 5 km west of a normal faulting event. Both results are of quality (A). The downdip termination of thrust events can be accurately traced in map view. It approximately follows the eastern flank of the trench-parallel Coastal Cordillera (Figure 2).

Beyond and below the thrust zone, that is, in the lower band, in the transitional zone, and in the strong cluster, σ_1 rotates to slab normal and seismicity becomes dominated by normal faulting. σ_3 is directed approximately slab parallel in convergence direction (*C* in Figure 3) and σ_2 strike parallel (Figures 3 and 4). A general trend exists along the subduction pathway: Starting in the lower band, faulting styles are more heterogeneous and Φ is low (supporting information S4) indicating that the magnitudes of σ_2 and σ_3 are similar. Accordingly the directions of σ_2 and σ_3 have a large uncertainty in the slab plane. *T* axes scatter broadly ±30° around the slab plane and have an azimuth that loosely follows the convergence direction (*DE* in Figure 3). Further downdip,

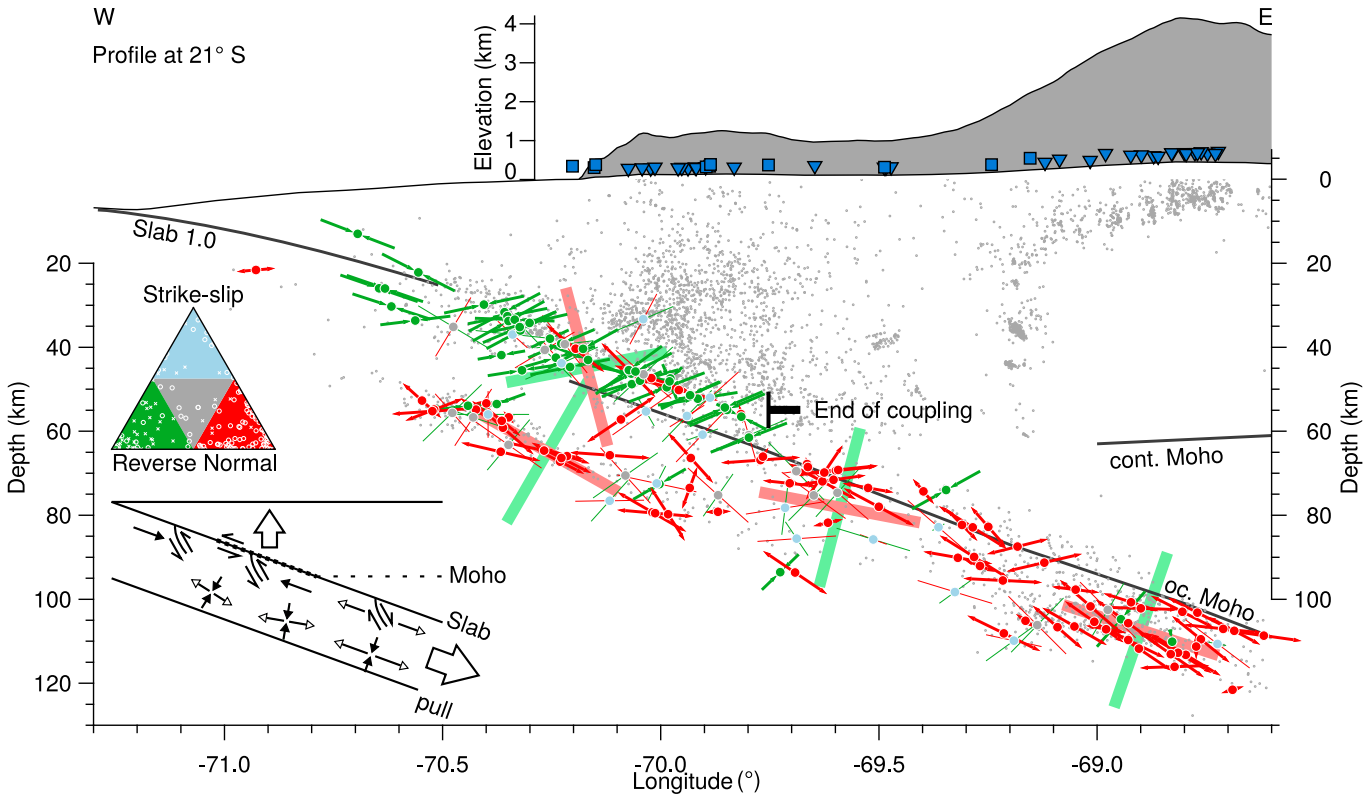

Figure 4. (top) Exaggerated average elevation in the study area. (bottom) Profile view of the seismicity distribution, color coded by faulting style (Frohlich, 1992) as thrust (green), normal (red), strike-slip (light blue), or odd faults (gray). Projection of the *P* axes for thrust faults (green arrows), *T* axes for normal faults (red arrows) or both for strike-slip and odd faults (thin streaks). Direction of σ_1 (light green bars) and σ_3 (light red bars). Slab 1.0 model (Hayes et al., 2012). Receiver function Moho (Yuan et al., 2000). Inset: Interpretational sketch of the activated structures and schematic relative main stress components (see section 5 for details).

in the transitional zone, the *T* axes pattern is similar, but Φ becomes larger and the σ_2 and σ_3 directions are better defined (Figure 3). Finally, in the strong cluster, the σ_3 direction aligns sharply with the downdip convergence direction and *T* axes align with the slab plane (Figures 3 and 4).

In the normal faulting regime a second trend exists across the slab. Earthquakes that occur at a perpendicular separation distance $\lesssim$12 km from the slab surface (outlined orange red in Figures 1–3) tend to have their *T* axes oriented away from the σ_3 direction (but in the slab plane) and the *N* axes close to horizontal. In contrast to that, earthquakes $\gtrsim$12 km from the slab surface have *T* axes that tend to follow the σ_3 direction and *N* axes that may be oriented more vertically.

4. Interpretation

The sharp separation between the compressional and the extensional regime occurs at the downdip end of interface seismicity (Figure 4), indicating that this line is the downdip end of interplate coupling. Updip of this line, the upper part of the slab is in compression, which we interpret in the sense that both plates converge, collisional forces act on the subducting plate and affect the entire oceanic crust: The plate interface is interseismically coupled, the continent acts as a backstop, and stress becomes transferred to the overriding plate. Slip deficit along the plate interface accumulates only until the downdip end of seismic coupling, limiting the maximum extent of a complete megathrust rupture and therefore the maximum earthquake magnitude. Uplift of the Coastal Cordillera and seismicity in the continental crust likely happen in response to these stresses. The interface thrust earthquakes represent localized decoupling events that activate the plate interface. These events occur in the deepest part of the seismogenic zone, which is not fully coupled and likely characterized by heterogeneous frictional properties (Lay et al., 2012; Schurr et al., 2012).

The remainder of the focal mechanisms in the coupling zone may represent the reactivation of bend faults, as has been suggested by Ranero et al. (2005). In fact, outer rise bend faults that have been identified using

high-resolution bathymetry off the coast of northern Chile between 22°S and 24°S have two dominant directions, one NNE striking and one NW striking (Ranero et al., 2005). The *N* axes, which are the intersections of both nodal planes, scatter near horizontally around this set of directions (*NW* and *NNE* in Figure 3), consistent with an activation of either of the nodal planes with slip in fault dip direction.

Below the downdip end of interplate coupling normal faulting becomes ubiquitous. The slab is under tension, which is due to the stress field being dominated by mantle side slab pull there. The change in stress regime occurs at the point, where also the reflectivity response of the plate interface broadens characteristically to form a few kilometer thick reflection band (Bloch et al., 2014; Yoon et al., 2008). In northern Cascadia, a similar structure has earlier been interpreted as representing the transition from a coupled to a creeping plate interface (Nedimovic et al., 2003).

The sharp alignment of the σ_3 direction and the *T* axes with the downdip convergence vector in the strong seismicity cluster likely indicates that the relative contribution of slab pull to the stress field increases below 100-km depth.

The trend of *T* axes being oriented away from the σ_3 direction nearer to the slab surface (orange red in Figures 1–3) may indicate that the orientation of focal mechanisms there is controlled structurely, that is, by faults and weakness zones that have variable orientations. In contrast to that, further away from the slab surface, where *T* axes align with σ_3, the faulting angle is more likely controlled by the orientation of the stress field, within an unstructured or virgin rock.

5. Discussion

The general pattern of the plate interface becoming activated in numerous small reverse faulting earthquakes at shallow depth and slab pull becoming the dominant forcing at intermediate depth is consistently observed in double and triple seismic zones in Japan (Igarashi et al., 2001; Kita et al., 2010), New Zealand (Reyners et al., 1997), and Taiwan (Kao & Rau, 1999). The sharp downdip end of interface coupling has been observed in Japan (Igarashi et al., 2001; Kita et al., 2010). In the Central Andean subduction zone it has been inferred from the occurrence of interface aftershock seismicity (Schurr et al., 2012) and from thermal and structural modeling (Oleskevich et al., 1999). Our study indicates that a similar abrupt change in stress regime as in Japan occurs in the Central Andean forearc. The location is consistent with the probable intersection of the slab with continental Moho, which indicates that the downdip extent of interplate coupling is likely controlled by the change in upper plate rheology.

The observation that *T* axes align with the slab dip going to greater depth has been made by Delouis et al. (1996) beyond the coupling zone. Our data show that this pattern continues also below the coupling zone in the previously not observed lower seismicity plane. The observation that *T* axes align with the downdip convergence direction deeper below the slab surface has been made by Rietbrock and Waldhauser (2004) in the strong seismicity cluster. We can confirm that this pattern also affects the transitional part of the slab between the coupling zone and the strong seismicity cluster. This makes us confident that these observations are significant and probably related to slab structure and stressing in general.

Ranero et al. (2005) argue that many intermediate depth earthquakes could occur on reactivated outer rise bend faults, because their bathymetrically mapped strike shows a strong similarity to the one of moment tensors in the corresponding trench segment at intermediate depth. Rietbrock and Waldhauser (2004) draw the same conclusion from the subvertical alignment of fine seismic structures and subvertical nodal planes of intermediate depth earthquakes in the Central Andes. Our data suggest that the reactivation of bend faults is likely for seismicity down to 12 km below the slab interface (orange red in Figures 2 and 3). The focal mechanisms whose *T* axes lie close to the σ_3 direction which are more concentrated further away from the slab surface more likely represent spontaneous faulting of the relatively undisturbed rock in the prevailing local stress field. Faulting of undisturbed rocks at high confining pressures would likely be assisted by metamorphic mineral reactions (e.g., Ferrand et al., 2017; Jung et al., 2004; Peacock, 2001; Proctor & Hirth, 2015), which would advance in directions that are prescribed by local stresses and so could cause the observed faulting pattern.

The proposed increase of the slab pull component below 100-km depth may indicate that the slab pull stresses are not fully transferred to the updip part and/or that an additional stress component exists in the forearc that opposes mantle side slab pull.

Incomplete stress transfer is generally to be expected, because some stress drop and dissipation of elastic energy occur evidently in every single intermediate depth earthquake or more subtle by aseismic deformation. There is also evidence for stresses that oppose slab pull: The unbending of the slab requires it to be buoyant in the forearc region. The interpretation that the strong seismicity cluster is the locus of major slab devolatilization corroborates this, because the updip part of the slab would need to be hydrated and therefore may have a relatively low density. Furthermore, the alignment of the σ_3 direction and the *T* axes occurs just before the point where the slab becomes transparent on receiver function images (Wölbern et al., 2009; Yuan et al., 2000) and where its dip angle steepens significantly (Sippl et al., 2018). Both phenomena are thought to be related to the metamorphic transformation of the slab material from less dense blueschist (crust) and serpentinized peridotite (mantle) to denser eclogite and harzburgite. Slab buoyancy would oppose slab pull and the densification from a buoyant to a sinking slab would manifest itself in the *T* axes pattern that we observe.

The increase of the slab pull component that we propose here would likely also be the cause for the increase in event rate along the subduction pathway and the occurrence of strong intermediate depth earthquakes in the past, like the M_w7.7, 2005 Tarapacá earthquake (Delouis & Legrand, 2007; Peyrat et al., 2006) or the M_s8, 1950 Atacama earthquake (Kausel & Campos, 1992). They had similar source mechanisms like those that we determined for the earthquakes in the strong cluster that are farthest away from the plate interface. Our interpretation that these earthquakes rupture virgin or unstructured rock would be in agreement with a large stress drop and subhorizontal fault plane that has been reported for the Tarapacá earthquake (Peyrat et al., 2006). Similar $M > 7$ intermediate depth earthquakes have been reported in the subduction zone of Japan (Suzuki & Kasahara, 1996).

6. Conclusion

We determined focal mechanisms of earthquakes that occurred within the subducting Nazca slab and on its interface to the overriding South American plate. We could sample the slab continuously from 20- to 120-km depth, in its crust and mantle. Focal mechanisms indicate an abrupt change in stress regime along a line that approximately correlates with the eastern extent of the Coastal Cordillera. Updip of this line lies the coupling zone, where compressional stresses prevail due to plate convergence and earthquakes activate the partially coupled plate interface and likely intraplate outer rise bend faults. This line marks the maximal downdip extent of great megathrust earthquakes, limiting their magnitude. Beyond and below the coupling zone, the stress regime is controlled by slab pull. Along the subduction pathway we find a pronounced alignment of *T* axes and the σ_3 direction with the slab plane and an increased dominance of normal faulting, which we interpret in the sense that the effect of slab pull increases. The updip parts of the slab might be less affected by slab pull, because of dissipation of elastic energy and/or due to slab buoyancy. Additionally, the tendency of *T* axes to be oriented away from the σ_3 direction near the slab surface likely indicates that fault orientation there is controlled by inherited structures, likely outer rise bend faults. Deeper within the subducting plate, earthquakes more likely rupture predominantly unstructured or virgin rock, likely assisted by metamorphic mineral reactions. In the deepest part, where strong slab pull stresses act on the potentially unstructured rock fabric, the potential for large intermediate depth earthquakes arises.

Acknowledgments
This work has been funded by Deutsche Forschungsgemeinschaft research grant Ku 2484/2-1. Seismic waveform data (Wigger et al., 2016; GFZ, and IPGP, 2006) are available via the GEOFON server. Part of the instruments were provided by GIPP of GFZ Potsdam. Seismic data were processed using obspy (Krischer et al., 2015). All figures have been prepared using Generic Mapping Tools (Wessel et al., 2013) and other free software.

References

Angermann, D., Klotz, J., & Reigber, C. (1999). Space-geodetic estimation of the Nazca-South America Euler vector. *Earth and Planetary Science Letters*, *171*(3), 329–334.

Bloch, W., Kummerow, J., Salazar, P., Wigger, P., & Shapiro, S. A. (2014). High-resolution image of the North Chilean subduction zone: Seismicity, reflectivity and fluids. *Geophysical Journal International*, *197*, 1744–1749. https://doi.org/10.1093/gji/ggu084

Bouchon, M. (1981). A simple method to calculate Green's functions for elastic layered media. *Bulletin of the Seismological Society of America*, *71*(4), 959–971.

Comte, D., Dorbath, L., Pardo, M., Monfret, T., Haessler, H., Rivera, L., et al. (1999). A double-layered seismic zone in Arica, northern Chile. *Geophysical Research Letters*, *26*(13), 1965–1968.

Comte, D., & Pardo, M. (1991). Reappraisal of great historical earthquakes in the northern Chile and southern Peru seismic gaps. *Natural Hazards*, *4*(1), 23–44.

Comte, D., & Suarez, G. (1994). An inverted double seismic zone in Chile: Evidence of phase transformation in the subducted slab. *Science*, *263*, 212–215.

Delouis, B., Cisternas, A., Dorbath, L., Rivera, L., & Kausel, E. (1996). The andean subduction zone between 22 and 25 s (northern chile): Precise geometry and state of stress. *Tectonophysics*, *259*(1-3), 81–100.

Delouis, B., & Legrand, D. (2007). Mw 7.8 Tarapaca intermediate depth earthquake of 13 June 2005 (northern Chile): Fault plane identification and slip distribution by waveform inversion. *Geophysical Research Letters*, *34*, L01304. https://doi.org/10.1029/2006GL028193

Delouis, B., Pardo, M., Legrand, D., & Monfret, T. (2009). The Mw 7.7 Tocopilla earthquake of 14 November 2007 at the southern edge of the northern Chile seismic gap: Rupture in the deep part of the coupled plate interface. *Bulletin of the Seismological Society of America*, *99*(1), 87–94.

Ferrand, T. P., Hilairet, N., Incel, S., Deldicque, D., Labrousse, L., Gasc, J., et al. (2017). Dehydration-driven stress transfer triggers intermediate-depth earthquakes. *Nature Communications*, *8*(15), 247.

Frohlich, C. (1992). Triangle diagrams: Ternary graphs to display similarity and diversity of earthquake focal mechanisms. *Physics of the Earth and Planetary Interiors*, *75*(1-3), 193–198.

GFZ, and IPGP (2006). IPOC seismic network, integrated plate boundary observatory Chile. https://doi.org/10.14470/ PK615318, other/Seismic Network.

Gephart, J. W., & Forsyth, D. W. (1984). An improved method for determining the regional stress tensor using earthquake focal mechanism data: Application to the San Fernando earthquake sequence. *Journal of Geophysical Research*, *89*(B11), 9305–9320.

Hardebeck, J. L., & Shearer, P. M. (2002). A new method for determining first-motion focal mechanisms. *Bulletin of the Seismological Society of America*, *92*, 2264–2276.

Hardebeck, J. L., & Shearer, P. M. (2003). Using S/P amplitude ratios to constrain the focal mechanisms of small earthquakes. *Bulletin of the Seismological Society of America*, *93*, 2434–2444.

Hayes, G. P., Herman, M. W., Barnhart, W. D., Furlong, K. P., Riquelme, S., Benz, H. M., et al. (2014). Continuing megathrust earthquake potential in Chile after the 2014 Iquique earthquake. *Nature*, *512*(7514), 295–298.

Hayes, G. P., Wald, D. J., & Johnson, R. L. (2012). Slab1. 0: A three-dimensional model of global subduction zone geometries. *Journal of Geophysical Research*, *117*, B01302. https://doi.org/10.1029/2011JB008524

Husen, S., Kissling, E., Flueh, E., & Asch, G. (1999). Accurate hypocentre determination in the seismogenic zone of the subducting Nazca plate in northern Chile using a combined on-/offshore network. *Geophysical Journal International*, *138*(3), 687–701.

Igarashi, T., Matsuzawa, T., Umino, N., & Hasegawa, A. (2001). Spatial distribution of focal mechanisms for interplate and intraplate earthquakes associated with the subducting Pacific plate beneath the northeastern Japan arc: A triple-planed deep seismic zone. *Journal of Geophysical Research*, *106*, 2177–2191.

Jost, M. u., & Herrmann, R. (1989). A students guide to and review of moment tensors. *Seismological Research Letters*, *60*(2), 37–57.

Jung, H., Green Ii, H. W., & Dobrzhinetskaya, L. F. (2004). Intermediate-depth earthquake faulting by dehydration embrittlement with negative volume change. *Nature*, *428*(6982), 545–549.

Kao, H., & Rau, R.-J. (1999). Detailed structures of the subducted Philippine Sea Plate beneath northeast Taiwan: A new type of double seismic zone. *Journal of Geophysical Research*, *104*(B1), 1015–1033.

Kausel, E., & Campos, J. (1992). The $Ms = 8$ tensional earthquake of 9 December 1950 of northern Chile and its relation to the seismic potential of the region. *Physics of the Earth and Planetary Interiors*, *72*(3-4), 220–235.

Kita, S., Okada, T., Hasegawa, A., Nakajima, J., & Matsuzawa, T. (2010). Existence of interplane earthquakes and neutral stress boundary between the upper and lower planes of the double seismic zone beneath Tohoku and Hokkaido, northeastern Japan. *Tectonophysics*, *496*(1), 68–82.

Krischer, L., Megies, T., Barsch, R., Beyreuther, M., Lecocq, T., Caudron, C., & Wassermann, J. (2015). Obspy: A bridge for seismology into the scientific python ecosystem. *Computational Science & Discovery*, *8*(1), 014003.

Kumar, A., Wagner, L. S., Beck, S. L., Long, M. D., Zandt, G., Young, B., et al. (2016). Seismicity and state of stress in the central and southern Peruvian flat slab. *Earth and Planetary Science Letters*, *441*, 71–80.

Lay, T., Kanamori, H., Ammon, C. J., Koper, K. D., Hutko, A. R., Ye, L., et al. (2012). Depth-varying rupture properties of subduction zone megathrust faults. *Journal of Geophysical Research*, *117*, B04311. https://doi.org/10.1029/2011JB009133

Lüth, S. (2000). Ergebnisse weitwinkelseismischer Untersuchungen und die Struktur der Kruste auf einer Traverse über die zentralen Anden bei 21° S. *Berliner geowiss Abh*, *37*.

Métois, M., Socquet, A., Vigny, C., Carrizo, D., Peyrat, S., Delorme, A., et al. (2013). Revisiting the North Chile seismic gap segmentation using GPS-derived interseismic coupling. *Geophysical Journal International*, *194*, 1283–1294. https://doi.org/10.1093/gji/ggt183

Michael, A. J. (1987). Use of focal mechanisms to determine stress: A control study. *Journal of Geophysical Research*, *92*(B1), 357–368.

Nábělek, J., & Xia, G. (1995). Moment-tensor analysis using regional data: Application to the 25 March, 1993, Scotts Mills, Oregon, Earthquake. *Geophysical Research Letters*, *22*(1), 13–16.

Nedimovic, M. R., Hyndman, R. D., Ramachandran, K., & Spence, G. D. (2003). Reflection signature of seismic and aseismic slip on the northern Cascadia subduction interface. *Nature*, *424*, 416–420. https://doi.org/10.1038/nature01840

Oleskevich, D., Hyndman, R., & Wang, K. (1999). The updip and downdip limits to great subduction earthquakes: Thermal and structural models of Cascadia, south Alaska, SW Japan, and Chile. *Journal of Geophysical Research*, *104*(B7), 14,965–14,991.

Oncken, O., Asch, G., Haberland, C., Metchie, J., Sobolev, S., Stiller, M., et al. (2003). Seismic imaging of a convergent continental margin and plateau in the central Andes (Andean continental research project 1996 (ANCORP'96)). *Journal of Geophysical Research*, *108*(B7), 2328. https://doi.org/10.1029/2002JB001771

Oncken, O., Lüschen, E., Mechie, J., Sobolev, S., Schulze, A., Gaedicke, C., et al. (1999). Seismic reflection image revealing offset of Andean subduction-zone earthquake locations into oceanic mantle. *Nature*, *397*(6717), 341.

Peacock, S. M. (2001). Are the lower planes of double seismic zones caused by serpentine dehydration in subducting oceanic mantle? *Geology*, *29*(4), 299–302.

Peyrat, S., Campos, J., De Chabalier, J.-B., Perez, A., Bonvalot, S., Bouin, M.-P., et al. (2006). Tarapacá intermediate-depth earthquake (Mw 7.7, 2005, northern Chile): A slab-pull event with horizontal fault plane constrained from seismologic and geodetic observations. *Geophysical Research Letters*, *33*, L22308. https://doi.org/10.1029/2006GL027710

Proctor, B., & Hirth, G. (2015). Role of pore fluid pressure on transient strength changes and fabric development during serpentine dehydration at mantle conditions: Implications for subduction-zone seismicity. *Earth and Planetary Science Letters*, *421*, 1–12.

Ranero, C. R., Morgan, J. P., McIntosh, K., & Reichert, C. (2003). Bending-related faulting and mantle serpentinization at the Middle America trench. *Nature*, *425*(6956), 367–373.

Ranero, C. R., Villaseñor, A., Phipps Morgan, J., & Weinrebe, W. (2005). Relationship between bend-faulting at trenches and intermediate-depth seismicity. *Geochemistry, Geophysics, Geosystems*, *6*, Q12002. https://doi.org/10.1029/2005gc000997

Reyners, M., Robinson, R., & McGinty, P. (1997). Plate coupling in the northern South Island and southernmost North Island, New Zealand, as illuminated by earthquake focal mechanisms. *Journal of Geophysical Research*, *102*(B7), 15,197–15,210.

Rietbrock, A., & Waldhauser, F. (2004). A narrowly spaced double-seismic zone in the subducting Nazca plate. *Geophysical Research Letters*, *31*, L10608. https://doi.org/10.1029/2004GL019610

Ruiz, S., Metois, M., Fuenzalida, A., Ruiz, J., Leyton, F., Grandin, R., et al. (2014). Intense foreshocks and a slow slip event preceded the 2014 Iquique Mw 8.1 earthquake. *Science*, *345*(6201), 1165–1169.

Schurr, B., Asch, G., Hainzl, S., Bedford, J., Hoechner, A., Palo, M., et al. (2014). Gradual unlocking of plate boundary controlled initiation of the 2014 Iquique earthquake. *Nature*, *512*(7514), 299–302.

Schurr, B., Asch, G., Rosenau, M., Oncken, O., Barrientos, S., Salazar, P., & Vilotte, J.-P. (2012). The 2007 M7.7 Tocopilla northern Chile earthquake sequence: Implications for along-strike and downdip rupture segmentation and megathrust frictional behavior. *Journal of Geophysical Research*, *117*, B05305. https://doi.org/10.1029/2011JB009030

Schurr, B., & Nábělek, J. (1999). New techniques for the analysis of earthquake sources from local array data with an application to the Scotts Mills, Oregon, aftershock sequence. *Geophysical Journal International*, *137*(3), 585–600.

Sippl, C., Schurr, B., Asch, G., & Kummerow, J. (2018). Seismicity structure of the northern Chile forearc from > 100,000 double-difference relocated hypocenters. *Journal of Geophysical Research: Solid Earth*, *123*. https://doi.org/10.1002/2017JB015384

Suzuki, S., & Kasahara, M. (1996). Unbending and horizontal fracture of the subducting Pacific plate, as evidenced by the 1993 Kushiro-oki and the 1981 and 1987 intermediate-depth earthquakes in Hokkaido. *Physics of the Earth and Planetary Interiors*, *93*(1-2), 91–104.

Wessel, P., Smith, W. H., Scharroo, R., Luis, J., & Wobbe, F. (2013). Generic mapping tools: Improved version released. *Eos, Transactions American Geophysical Union*, *94*(45), 409–410.

Wigger, P., Salazar, P., Kummerow, J., Bloch, W., Asch, G., & Shapiro, S. (2016). West-fissure- and Atacama-fault seismic network (2005/2012) https://doi.org/10.14470/3S7550699980, other/Seismic Network.

Wölbern, I., Heit, B., Yuan, X., Asch, G., Kind, R., Viramonte, J., et al. (2009). Receiver function images from the moho and the slab beneath the Altiplano and Puna plateaus in the central Andes. *Geophysical Journal International*, *177*(1), 296–308.

Yoon, M., Buske, S., Shapiro, S., & Wigger, P. (2008). Reflection image spectroscopy across the Andean subduction zone. *Tectonophysics*, *472*, 51–61. https://doi.org/10.1016/j.tecto.2008.03.14

Yuan, X., Sobolev, S. V., Kind, R., Oncken, O., Bock, G., Asch, G., et al. (2000). Subduction and collision processes in the Central Andes constrained by converted seismic phases. *Nature*, *408*, 958–961.